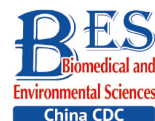


Original Article

**SET8 Inhibition Potentiates Radiotherapy by Suppressing DNA Damage Repair in Carcinomas***

PAN Dong^{1,2,3}, DU Ya Rong², LI Rong¹, SHEN Ai Hua¹, LIU Xiao Dong¹,
LI Chuan Yuan³, and HU Bu Rong^{1,2,#}

1. Department of Radiological Health and Radiation Medicine, School of Public Health and Management, Wenzhou Medical University, Wenzhou 325035, Zhejiang, China; 2. Key Laboratory of Heavy Ion Radiation Biology and Medicine of Chinese Academy of Sciences & Key laboratory of Space Radiobiology of Gansu province, Institute of Modern Physics, Chinese Academy of Sciences, Lanzhou 730000, Gansu, China; 3. Department of Dermatology, Duke University Medical Center, Durham, NC, 27710, USA

Abstract

Objective SET8 is a member of the SET domain-containing family and the only known lysine methyltransferase (KMT) that monomethylates lysine 20 of histone H4 (H4K20me1). SET8 has been implicated in many essential cellular processes, including cell cycle regulation, DNA replication, DNA damage response, and carcinogenesis. There is no conclusive evidence, however, regarding the effect of SET8 on radiotherapy. In the current study we determined the efficacy of SET8 inhibition on radiotherapy of tumors and the underlying mechanism.

Methods First, we explored the radiotherapy benefit of the SET8 expression signature by analyzing clinical data. Then, we measured a series of biological endpoints, including the xenograft tumor growth in mice and apoptosis, frequency of micronuclei, and foci of 53BP1 and γ -H2AX in cells to detect the SET8 effects on radiosensitivity. RNA sequencing and subsequent experiments were exploited to verify the mechanism underlying the SET8 effects on radiotherapy.

Results Low expression of SET8 predicted a better benefit to radiotherapy in lung adenocarcinoma (LUAD) and invasive breast carcinoma (BRCA) patients. Furthermore, genetic deletion of SET8 significantly enhanced radiation treatment efficacy in a murine tumor model, and A549 and MCF7 cells; SET8 overexpression decreased the radiosensitivity. SET8 inhibition induced more apoptosis, the frequency of micronuclei, and blocked the kinetics process of DNA damage repair as 53BP1 and γ -H2AX foci remained in cells. Moreover, RNF8 was positively correlated with the SET8 impact on DNA damage repair.

Conclusion Our results demonstrated that SET8 inhibition enhanced radiosensitivity by suppressing DNA damage repair, thus suggesting that SET8 potentiated radiotherapy of carcinomas. As new inhibitors of SET8 are synthesized and tested in preclinical and clinical settings, combining SET8 inhibitors with radiation warrants consideration for precise radiotherapy.

Key words: SET8; Histone methylation; DNA repair; Radiotherapy; Carcinoma

Biomed Environ Sci, 2022; 35(3): 194-205 doi: 10.3967/bes2022.028

ISSN: 0895-3988

www.besjournal.com (full text)

CN: 11-2816/Q

Copyright ©2022 by China CDC

INTRODUCTION

Lung cancer is one of the most frequently diagnosed cancers in terms of incidence and mortality, with approximately 1.38 million

deaths every year worldwide, while breast cancer is the most prevalent cancer globally among women^[1]. Radiotherapy is a widely utilized treatment modality for malignancies, especially in lung and breast cancer, but one of the main obstacles in these tumor

*This study was supported by the National Natural Science Foundation of China [U1432121, 11635013, 11705248].

#Correspondence should be addressed to HU Bu Rong, Tel: 86-577-86690971, E-mail: brhu@wmu.edu.cn

Biographical note of the first author: PAN Dong, male, born in 1988, PhD, majoring in biophysics.

types is radioresistance.

It is widely recognized that epigenetic dysregulation is an important mechanism underlying cancer development and progression. Histone post-translational modifications (PTMs), such as methylation, phosphorylation, acetylation, ubiquitination, and other epigenetic mechanisms, appear to function together in establishing and maintaining gene activity states, thus PTMs are essential for cell-fate determination and development^[2]. Histone methylation in a lysine or arginine residue is highly conserved as it acts in a coordinated and orderly fashion to regulate cellular processes, including gene transcription, DNA replication, and DNA repair^[3].

SET8, a member of the SET domain-containing family, is the only known lysine methyltransferase (KMT) that monomethylates lysine 20 of histone H4 (H4K20me1) *in vivo*^[4]. SET8 methyltransferase activity has been closely connected with carcinogenesis. SET8-mediated p53K382me1 suppresses p53-dependent transcription activation in cancer cells^[5]. SET8 degradation inhibits H4K20me1 and suppresses epithelial-mesenchymal transition (EMT) and invasion of breast cancer cells^[6]. SET8 has also been implicated in many essential cellular processes, including cell cycle regulation, DNA replication, and the DNA damage response^[7]. Moreover, disruption of endogenous SET8, accompanied by suppression of H4K20me1, leads to cell cycle defects, chromatin decondensation, and enlarged nuclei, indicating the essential role(s) of SET8 in DNA repair^[8-10]. Although the evidence regarding the impact of SET8 on radiation treatment is inconclusive, there is significant interest in the precise effect of SET8 on radiotherapy.

Our clinical data analysis suggested that low levels of SET8 contribute to radiotherapy efficacy in patients with lung adenocarcinoma (LUAD) and invasive breast carcinoma (BRCA). Single-cell RNA sequencing (ScRNA-seq) revealed that low SET8 expression is associated with a reduced capacity for DNA repair. To further elucidate our observations, we used the SET8-deficient A549 and MCF7 cell lines exposed to radiation. SET8 deficiency was shown to enhance radiosensitivity by blocking DNA damage repair.

MATERIALS AND METHODS

Patient Treatment and Clinical Data

All patient treatment and clinical data were

obtained from the cBioPortal database (<https://www.cbioportal.org>)^[11], which includes 32 studies consisting of approximately 10,000 specimens and representing 33 types of cancer from The Cancer Genome Atlas (TCGA)^[12]. Published clinical and genomic data from the TCGA PanCancer LUAD cohort, including 61 and 402 late-stage cancer patients treated and not treated with radiotherapy, respectively. Five hundred forty-eight and 433 cancer patients were included in the BRCA cohort who were treated and not treated with radiotherapy, respectively. Kaplan-Meier survival curves were generated using the statistical software, GraphPad Prism. The non-parametric Mantel-Cox log-rank test was used to determine the statistical differences among different patient groups. The Pearson correlation coefficients (*R*) of gene expression relevance were calculated by GraphPad Prism.

Cell Culture

A549 (human lung carcinoma), MCF7 (human breast carcinoma), LLC1 (mouse lung carcinoma), and HEK 293T cells (human embryonic kidney) were obtained from the American Type Culture Collection (Manassas, VA, USA). A549 cells were cultured in Ham's F-12K medium (Gibco, Waltham, MA, USA), and MCF7, LLC1, and HEK 293T cells were cultured in Dulbecco' Modified Eagle's Medium (DMEM; Gibco) supplemented with 10% (v/v) fetal bovine serum (FBS; Hyclone, Logan, UT, USA) and 1% penicillin/streptomycin. Cells were cultured at 37 °C in a humidified atmosphere containing 5% CO₂.

Radiation

X-ray irradiation was delivered in a Faxitron RX-650 system (100 kVp and 5 mA; Faxitron Bioptics, Marlborough, MA, USA) at room temperature. The target of this instrument is wolframium (W) and the dose was 0.76 Gy/min. Carbon ions irradiation (linear energy transfer [LET]: 80 KeV/μm) was delivered at the Heavy Ion Research Facility of Lanzhou, Institute of Modern Physics (HIRFL Lanzhou, China) with a dose of 0.4 Gy/min.

CRISPR/Cas9-mediated Gene Knockout of SET8

The knockout cells were generated using lentivirus-mediated CRISPR/Cas9 technology. Single guide RNA (sgRNA) sequences targeting human and mouse SET8 are listed in [Supplementary Table S1](#), available in www.besjournal.com. Double-stranded oligos encoding the sgRNA sequences were cloned into the BsmBI- (Thermal Fisher Scientific, Waltham, MA, USA) digested plasmid, LentiCRISPRv2

(deposited by Dr. Feng Zhang of MIT to Addgene, Watertown, MA, USA), which co-expresses Cas9 and sgRNA in the same vector. CRISPR lentivirus vectors were then produced in HEK 293T cells by psPAX2 and pMD2.G plasmids according to an established protocol by the Zhang laboratory^[13]. To generate the knockout cell lines, target cells were infected with lentivirus and selected in 1 µg/mL of puromycin.

SET8 overexpression and negative control vector were purchased from GeneCopoeia (Guangzhou, China). For transient transfection, cells were plated on the day before transfection at a confluence of 30%–50% performed with Lipofectamine 2000 (Invitrogen, Waltham, MA, USA) according to the manufacturer's instructions. The medium was replaced with fresh medium 6 h post-transfection. Cells were used in the following experiments after 48 h.

Western Blot

Cells were lysed in RIPA buffer (Beyotime, Shanghai, China) with protease inhibitor cocktail tablets (Roche, Basel, Basel-Stadt, Switzerland). Lysate total protein concentrations were determined using a protein assay kit (Bio-Rad, Hercules, CA, USA). Equal amounts of protein were denatured with loading buffer (Beyotime) at 100 °C for 10 min, then loaded onto a 10% SDS-PAGE gel for electrophoresis and transferred to a methanol-activated polyvinylidene fluoride membrane (Millipore, Burlington, MA, USA). The membrane was blocked in Tris-buffered saline (TBS) containing 5% bovine serum albumin (MP Biomedical, Solon, OH, USA) for 2 h at room temperature, then incubated with primary antibodies overnight at 4 °C. The following primary antibodies were used: SET8 (1:1,000, catalog No 14063-1-AP, Proteintech, Rosemont, IL, USA); RNF8 (1:1,000, catalog No. 14112-1-AP); H4K20me1 (1:1,000, catalog No. 9724; CST, Danvers, MA, USA); and GAPDH (1:2,000, catalog No. TA-08; ZSGB-BIO, Beijing, China). After twice-washing with TBS, the membranes were incubated with the appropriate horseradish peroxidase (HRP)-labeled secondary antibody for 1 h at room temperature. Secondary antibodies conjugated with HRP included goat anti-rabbit IgG (1:5,000, catalog No. ZB-2301; ZSGB-BIO). Immunoblots were visualized using an enhanced chemiluminescence (ECL) detection system (Thermal Fisher Scientific) according to the manufacturer's protocol, and autoradiography.

Tumor Growth Delay in Irradiated Mice

The animal experiments conducted in this study

were approved by the Wenzhou Medical University Institutional Animal Use and Care Committee. C57BL/6J mice were purchased from Beijing Vital River Laboratory Animal Technology Co., Ltd. (Beijing, China). Prior to tumor cell injection, the right hindlimbs of age-matched 6-week-old female mice were shaved. LLC1 cells (2×10^5) were resuspended in 50 µL of PBS and injected subcutaneously into the shaved flanks with vector control or SET8 knockout tumor cells. After 7 days, tumors were X-irradiated using lead shielding with a single 8 Gy dose. Tumor volumes were measured every other day and calculated using the following formula: $(\text{length}) \times (\text{width})^2/2$. The mice were sacrificed when tumor volumes reached 2,000 mm³. The Kaplan-Meier estimator and log-rank (Mantel-Cox) test were used for survival analysis among different tumor-bearing mice groups.

Clonogenic Survival Assay

After irradiation, cells were washed with PBS buffer, trypsinized, and counted using a cell counter (Beckman, Indianapolis, IN, USA). An appropriate number of cells (0 Gy: 100; 1 Gy: 200; 2 Gy: 500; 4 Gy: 2,000; 6 Gy: 10,000) were seeded into each Φ60 dish in 5 mL of complete media. After 10 days of incubation, colonies were fixed with 10 mL of fresh Carnoy's fluid and stained with 0.5% crystal violet for 20 min^[14]. Colonies with > 50 remaining cells were recorded and counted manually under an inverted microscope. Plating efficiencies (PEs) were calculated as follows: number of colonies formed/number of cells plated. Survival ratios were calculated as follows: numbers of colonies formed/numbers of cells plated. Cell surviving fractions were calculated as follows: PE (irradiated)/PE (non-irradiated).

Micronucleus Assay

The micronucleus test is used in toxicologic screening for potential genotoxic targets^[15]. Forty-eight hours after 4 Gy X-irradiation, cells were fixed with Carnoy's fluid for 20 min at room temperature and stained with 20 µL of acridine orange in an aqueous solution (10 µg/mL). Micronuclei identification was established by the following criteria: diameter less than one-third of the primary nucleus; and color is the same as or lighter than the main nucleus^[16]. Analyses were performed with an Axio Imager Z2 fluorescence microscope (Zeiss, Oberkochen, Germany) at 20 × magnification. At least 500 cells were scored for each sample.

Flow Cytometry Analysis of Apoptosis

Apoptosis was evaluated using an Annexin V-fluorescein isothiocyanate (FITC) and propidium iodide (PI) Apoptosis Detection Kit (Solarbio, Beijing, China) according to the manufacturer's instructions. Forty-eight hours after 4 Gy X-irradiation, the culture medium was removed and the wells were washed with PBS, then the cells were harvested by trypsinization and resuspended in binding buffer at 1×10^6 cells/mL and stained with Annexin V-FITC and PI on ice for 15 min in the dark. Cell fluorescence was examined with an ImageStream100 (Amnis, Austin, TX, USA).

Single-cell RNA Sequencing Analysis

Single-cell RNA sequencing analyses were performed using the CancerSEA database (<http://biocc.hrbmu.edu.cn/CancerSEA>), which is a cancer single-cell functional state atlas, involving 14 functional states of 41,900 single cancer cells from 25 cancer types^[17]. The scores of 14 functional states, including DNA repaired across single cancer cells in each dataset, were evaluated using gene set variation analysis (GSVA). The cohorts analyzed include LUAD and BRCA single-cell RNA sequencing data, which were retrieved from published studies^[18–21]. A non-parametric *t*-test was used to determine the statistical differences among different single-cell groups.

Quantitative Real-time Polymerase Chain Reaction (qRT-PCR)

Extraction of total RNA from cells was performed using the E.Z.N.A.® Total RNA Kit (Omega, Norcross, GA, USA) following the manufacturer's protocol. Reverse transcription was performed with the Transcriptor First Strand cDNA Synthesis Kit (Roche) and qRT-PCR was performed using SYBR Green PCR Master (Roche) to measure mRNA expression. The SET8 and GAPDH (internal control) primers were purchased from GeneCopoeia. The primers used for different genes are listed in [Supplementary Table S2](#), available in www.besjournal.com. qRT-PCR was performed on samples using the Chromo4 System Real-Time PCR detector (Bio-Rad, USA). All procedures were performed according to the manufacturers' protocols under the following conditions: initiation for 10 min at 95 °C; and 40 thermal cycles each at 95 °C for 10 s, 60 °C for 20 s, and 70 °C for 10 s. Relative fold-change in mRNA expression was calculated using the $2^{-\Delta\Delta Ct}$ method with the following equation: relative quantitation (RQ) = $2^{-\Delta\Delta Ct}$.

Immunostaining

To detect 53BP1 and γ -H2AX foci that formed at the DSB sites and the level of RNF8 expression, cells were seeded at 1×10^4 on glass coverslips in each well of a 12-well tissue culture plate and cultured for 24 h prior to being irradiated according to the experimental requirements. Subsequent experimental procedures were as previously described^[22]. After 1 Gy X-irradiation, cells were fixed with 4% paraformaldehyde (PFA) for 20 min at room temperature and permeabilized with 0.5% Triton X-100 in PBS while on ice for 10 min. Non-specific binding sites were blocked with 5% bovine serum albumin (BSA) in PBS for 60 min at room temperature prior to probing with primary antibodies. The primary antibodies used for immunostaining included RNF8 (1:500), 53BP1 (1:3,000, catalog No. ab36823; Abcam, Cambridge, MA, USA), and γ -H2AX (1:1,000, catalog No. 80312; CST). Secondary antibodies (anti-mouse or rabbit conjugated with Alexa 488/647) were purchased from Beyotime (1:2,000, catalog Nos. A0423 and A0473, respectively). Then, the cells were incubated in the primary antibody diluted in 5% BSA/1 \times PBS 1 h at room temperature. After incubation, cells were thrice-washed with PBS for 10 min each, then incubated with the appropriate Alexa Fluor secondary antibodies diluted in 5% BSA for 1 h. The cells were thrice-washed with PBS again for 10 min each. The nuclei were counterstained with DAPI (Beyotime). Digital image analysis was performed to determine the fluorescence intensity of RNF8 and the number of γ H2AX and 53BP1 foci using an Axio Imager Z2 fluorescence microscope at 63 \times magnification and confirmed by visual inspection of images. Quantification of fluorescence intensity or foci per cell was determined from images of 50 cells for every time point from at least three independent experiments.

RNA Sequencing and Analysis

For RNA sequencing, samples were collected, snap-frozen, and maintained at -80 °C prior to RNA extraction. Total RNA was extracted with TRIzol reagent (Invitrogen). Sequencing was performed using the Illumina sequencing platform (Majorbio Co., Shanghai, China). The measured data were mapped to reference genomes after quality control. After counting the reads mapped on the gene and calculating the gene expression, the differences in gene expression were analyzed.

Statistics

All *in vitro* experiments were performed in

triplicate and repeated at least three times. Statistical significance (P values) of differences in means between two samples were evaluated using unpaired t -tests. Data are represented as individual values or as the mean \pm sem. Group sizes (n) and applied statistical tests are indicated in the figure legends. For *in vivo* experiments and clinic data analysis, log-rank (Mantel-Cox) tests were used for survival analysis and tumor volume significances were assessed by two-way ANOVA among different groups. Statistics were calculated using GraphPad Prism 8.2.1. A $P < 0.05$ was considered statistically significant (*), $P < 0.01$ as highly significant (**), and $P < 0.001$ (***) as extremely significant.

RESULTS

Low SET8 Expression Predicts Benefits of Radiotherapy in LUAD and BRCA Patients

To determine the potential association between SET8 and radiotherapy in patients with cancer, we analyzed SET8 expression and efficacy of radiotherapy in LUAD and BRCA cancer patients known to have undergone radiotherapy^[11]. Our analysis indicated that LUAD patients with low SET8 expression had a significant advantage in overall survival (OS) when compared with high SET8 expression. Specifically, the median duration of OS was 45 and 26 months in the low and high SET8 expression groups, respectively ($P = 0.018$, log-rank test; [Figure 1A](#)). BRCA patients with low SET8 expression had a significantly better probability of progress-free survival (PFS) than the high-expression group; specifically, the median duration of PFS in the low-expression group was undefined compared to 146 months in the high-expression group ($P = 0.042$, [Figure 1B](#)). Importantly, the OS in the LUAD patients without radiotherapy was not significantly different between the SET8 low- and high-expression groups ($P = 0.41$, [Figure 1C](#)). Similarly, the PFS of BRCA patients without radiotherapy was not significantly different between the SET8 low- and high-expression groups ($P = 0.97$, [Figure 1D](#)).

Therefore, these data clearly demonstrated that low SET8 expression has significant advantages in cancer radiotherapy and it is directly responsible for the observed prognostic benefit in radiotherapy-treated patients among the TCGA PanCancer cohorts.

SET8 Alteration Affects Radiotherapy of Tumors both *in vivo* and *in vitro*

In consideration of low SET8 expression

benefiting radiotherapy, we hypothesized that SET8 deficiency sensitizes tumor cells to radiation. To confirm our hypothesis, we generated SET8 knockout LLC1 tumor cells using CRISPR/Cas9 ([Figure 2A](#)). Vector control and SET8 KO LLC1 cells were then used to establish subcutaneous tumors, which were then treated with 8 Gy of X-ray radiotherapy after 7 d. Our data indicated that SET8-deficient tumors grew slower than controls. Furthermore, SET8-deficient tumors responded to radiotherapy significantly better than vector controls ([Figure 2B](#)). Mice bearing SET8 KO tumors also survived significantly longer after radiotherapy ([Figure 2C](#)).

To evaluate the influence of SET8 on the intrinsic radiosensitivity of cancer cells, we generated SET8 knockout A549 and MCF7 cells using CRISPR/Cas9 ([Figure 2D](#)). We then performed a colony-forming assay after exposing the cells to different doses of X-rays. Our results indicated that SET8 deficiency significantly decreased the clonogenic abilities of A549 and MCF7 cells, especially at higher radiation doses ([Figure 2E–F](#)). Furthermore, the survival fraction increased significantly in the irradiated SET8 overexpression group compared with controls ([Figure 2G–I](#)).

We also measured the levels of SET8 and H4K20me1 expression in A549 cells exposed to low LET (X rays) and high LET (carbon ions, a promising radiotherapy particle) radiation at a series of time points using qRT-PCR and Western blotting, respectively (extended data, [Supplementary Figure S1](#), available in www.besjournal.com). Our results showed that SET8 and H4K20me1 expression decreased from 4–48 h in carbon ion X-irradiated A549 cells.

Taken together, these results indicate that SET8 expression alteration affected radiotherapy *in vivo* and *in vitro* and responded to ionizing radiation.

SET8 Expression Alteration Affects Radiation-induced Cellular Apoptosis and Nuclear Injury

Next, we attempted to determine if SET8 expression regulates radiation-induced cellular apoptosis and nuclear injury. [Figure 3A–B](#) show that SET8 knockout increased the proportion of radiation-induced apoptosis in A549 and MCF7 cells. Furthermore, SET8 knockout increased the frequency of micronuclei in irradiated cells ([Figure 3C–D](#)). Conversely, SET8 overexpression decreased the frequency of micronuclei ([Figure 3E–F](#)). These results further indicate that SET8 is positively

correlated with radiation resistance.

ScRNA-seq Analyses Reveal that SET8 is Associated with DNA Repair in LUAD and BRCA Patients

Further analysis of the role of SET8 in DNA repair was carried out utilizing ScRNA-seq to identify the mechanism underlying the SET8 increase in radiotherapy efficacy. The scores of DNA repaired across single cancer cells in each dataset were evaluated using the CancerSEA database. Comparing the SET8 low- and high-expression groups, there were significant positive correlations between SET8 expression and DNA repair scores in the two independent LUAD cohorts, including 126 and 42 samples, respectively (Figure 4A)^[18,19]. Similar results were obtained in the two independent BRCA cohorts

that included 369 and 70 samples (Figure 4B)^[20,21]. Thus, the above analyses proved that there is a positive association between SET8 expression and DNA repair.

SET8 Deficiency Blocks the process of DNA Damage Repair in A549 Cells

Because we have determined that SET8 expression is associated with DNA repair by ScRNA-seq, we subsequently speculated that SET8 inhibition enhanced radiotherapy by blocking the DNA damage repair process. To confirm this assumption, we directly visualized 53BP1 and γ H2AX foci, which are surrogate markers for DNA damage repair, by immunofluorescence. First, significantly lower numbers of 53BP1 and γ H2AX foci were observed

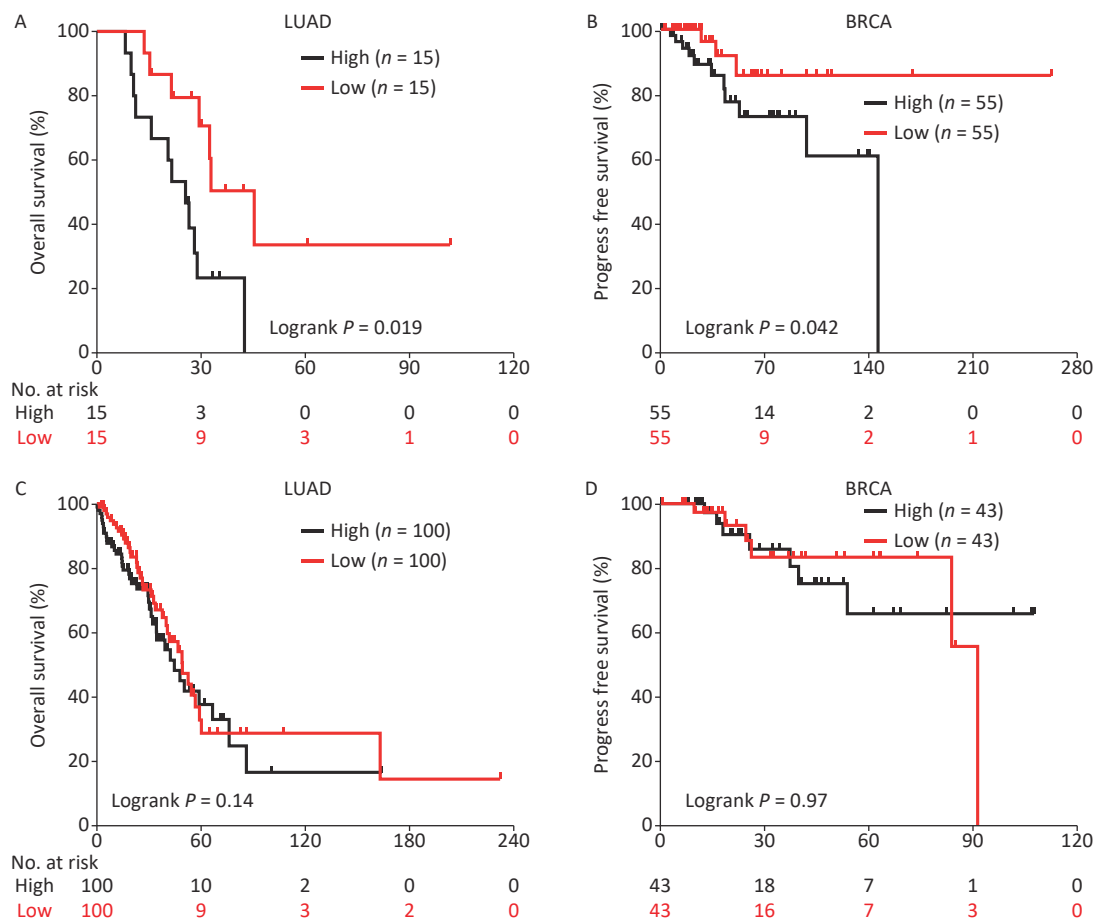


Figure 1. Kaplan-Meier survival curves of radiotherapy treated LUAD and BRCA patients with different SET8 expression. (A) Kaplan-Meier survival curves of radiotherapy-treated LUAD patients with low or high SET8 expression. (B) Kaplan-Meier survival curves of radiotherapy-treated BRCA patients with low or high SET8 expression. (C) Kaplan-Meier survival curves of radiotherapy untreated LUAD patients with low or high SET8 expression. (D) Kaplan-Meier survival curves of radiotherapy untreated BRCA patients with low or high SET8 expression. The cut-off values of high and low are top 25% and lowest 25% in LUAD, top 10% and lowest 10% in BRCA. P -values calculated by use of logrank test.

0.5 h after 1 Gy X-irradiation in SET8-deficient A549 cells (Figure 5). Further, the kinetics of foci dissolution of both two markers were delayed in SET8-deficient cells than in SET8-negative cells from 6–24 h. The above results indicated that SET8 deficiency hindered the recruitment of the DNA repair complex and DNA damage was refractory to repair in SET8-deficient A549 cells, which is consistent with previous reports^[6,7]. The above evidence suggests that SET8 deficiency blocked the

kinetics process of DNA damage repair.

SET8 Inhibition Reduced RNF8 Expression

We further investigated the functional connection between SET8 and other underlying genes to determine the mechanism underlying SET8-regulated radiotherapy efficacy. Before RNA sequencing, SET8 knockout and control A549 cells were exposed to 0 and 4 Gy of X-rays and collected 12 h after irradiation. Duplicate samples were in

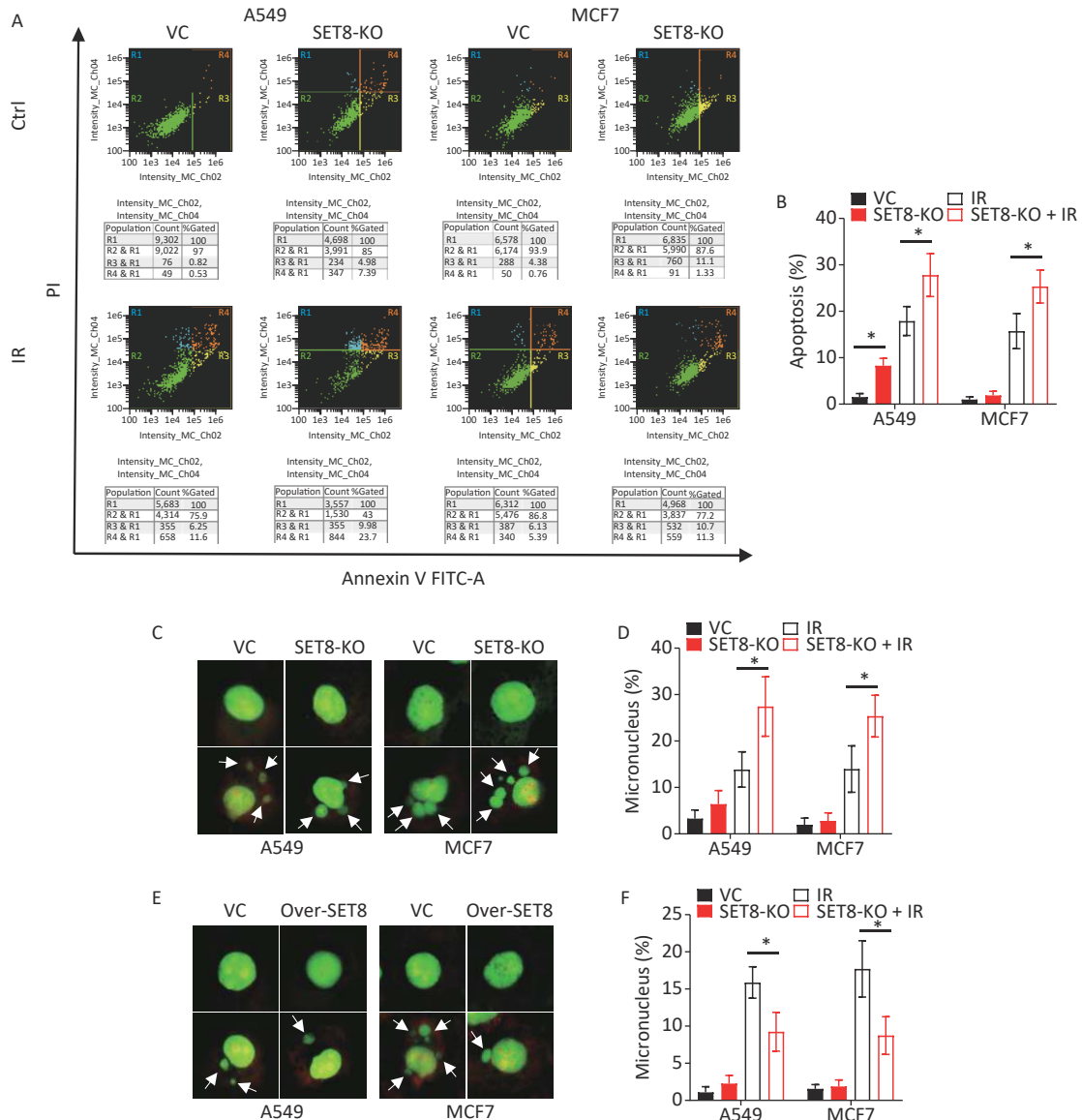


Figure 3. Cellular apoptosis and nucleus injury in irradiated SET8 alteration A549 and MCF7 cells. (A) & (B) Apoptosis proportion of SET8-KO or control A549 and MCF7 cells were exposed to 4 Gy X rays 48 h later. (C) & (D) Micronucleus frequency of SET8-KO or control A549 and MCF7 cells were exposed to 4 Gy X rays 48 h later. (E) & (F) Micronucleus frequency of Over-SET8 and control A549 and MCF7 cells were exposed to 4 Gy X rays 48 h later. Significance was determined by unpaired *t*-test. **P* < 0.05. IR, irradiation. VC, vector control.

each group for subsequent investigation. Gene expression relative fold-changes were calculated via RNA sequencing data. The set of 312 genes with > 2 fold-changes was analyzed using hierarchical clustering heatmap to reveal expression signatures (Figure 6A). Among the 312 genes, expression of 104 were significantly different between the SET8 knockout and control groups (43 were upregulated and 61 were downregulated; Figure 6B, Supplementary Table S3, available in www.besjournal.com). Ring finger protein 8 (RNF8) is involved in the aforementioned genes. RNF8 is an E3 ubiquitin (Ub) ligase with RING finger and has key roles in DNA damage and repair^[23]. Meanwhile, Zhou et al.^[22] reported that silencing of RNF8 enhances radiosensitivity in A549. Because RNF8 had persistent low expression in the SET8-KO groups that were independent of radiation by RNA sequencing, we explored the correlation between SET8 and RNF8. Figure 6C and d showed that the relative fluorescence intensity was low in the SET8 inhibition group. Our data further confirmed that RNF8 was downregulated in SET8 inhibition cells (Figure 6E). Above all, these results implied that SET8 inhibition induced radiation sensitization that depended on impeding RNF8 expression.

DISCUSSION

SET8 has been implicated in many essential cellular processes, including cell cycle regulation, DNA replication, and the DNA damage response.^[7]

There is no conclusive evidence about the contribution of SET8 to radiation treatment. The cBioPortal database provided abundant clinical data from TCGA, which provided the most direct evidence between genomic data and cancer prognosis in a variety of therapeutic strategies. Meanwhile, the genome-wide expression profiling of cancer tissues is an extremely useful method to explore the correlation of the genes *in vivo*^[11,12]. Our clinical and genomic data analysis in radiation-treated LUAD and BRCA patients offered theoretical proof that SET8 deficiency contributed to better radiotherapy efficiency. Subsequently, the current experiments clearly demonstrated that genetic deletion of SET8 significantly enhanced radiotherapy in a murine tumor model, and A549 and MCF7 cells *in vitro*, and SET8 overexpression was effective in decreasing radiosensitivity, which suggests the benefit of low SET8 expression to radiotherapy.

Emerging pieces of evidence have revealed that radiation-induced alterations in histone methylation affect the cellular response to radiation damage in the DNA^[24-29]. It is therefore important to characterize radiation-induced alterations in histone methylation patterns and the associated factors. Our study showed that ionizing radiation induced the recession of SET8 and H4K20me1 in the short term after irradiation. SET8/H4K20me1 oscillates during the cell cycle, and maintenance of H4K20me1 levels is critical for proper cell cycle progression through its role in protecting genome stability, DNA replication, mitosis, and transcription^[7], which indicates that

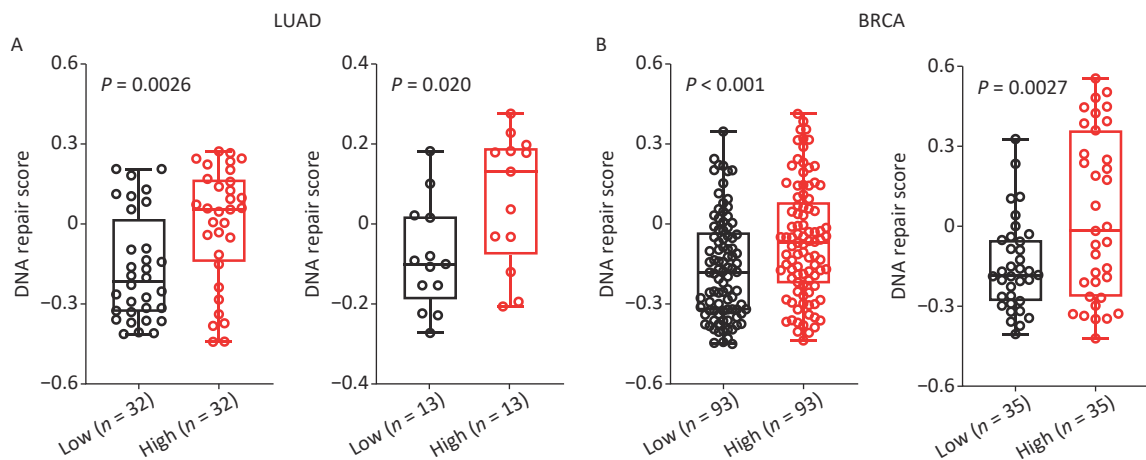


Figure 4. Single-cell RNA sequencing analyses between SET8 expression and DNA repair scores in LUAD and BRCA. (A) Scores of DNA repaired through single-cell RNA sequencing analyses in LUAD with SET8 expression low or high signature. (B) Scores of DNA repaired through single-cell RNA sequencing analyses in BRCA with SET8 expression low or high signature. The cut-off values of high and low are top 25% and lowest 25% in LUAD and BRCA. *P*-values calculated by use of unpaired *t*-test.

SET8/H4K20me1 may have an identical function in low and high LET radiation-induced DNA damage. SET8 directly modulates chromatin compaction and may be involved in the recruitment of signaling proteins, such as 53BP1, to the site of double-strand DNA breaks (DSBs)^[30,31]. Furthermore, when chromatin reorganization at DSBs is blocked, DNA repair is inhibited and cells exhibit increased sensitivity to radiation that creates DSBs^[32]. Our subsequent experiments revealed that SET8/H4K20me1 also affected radiosensitivity by blocking the kinetics process of DNA damage repair based on the reduction in 53BP1 and γ -H2AX foci.

RNF8 plays a key role in cellular life processes that promote the recruitment of several proteins,

such as 53BP1, Rad51, and BRCA1, at the sites of DNA damage by regulating the ubiquitination of H2AX to facilitate DNA repair. Previous studies have reported that aberrantly-expressed RNF8 may disrupt the DNA damage repair process^[33,34], especially in the A549 cells^[35]. Combined with our results, SET8 inhibition induced radiation sensitization involving the RNF8 pathway.

A series of inhibitors of SET8 or H4K20me1 have been synthesized and exhibit crucial biological functions in cell proliferation and DNA repair^[36–38]. SPS811–3 are small molecule inhibitors of SET8 that can result in cell-cycle defects at the S and G2/M phases, and the phenomenon can be recapitulated by RNAi-mediated knockdown of SET8^[36]. The

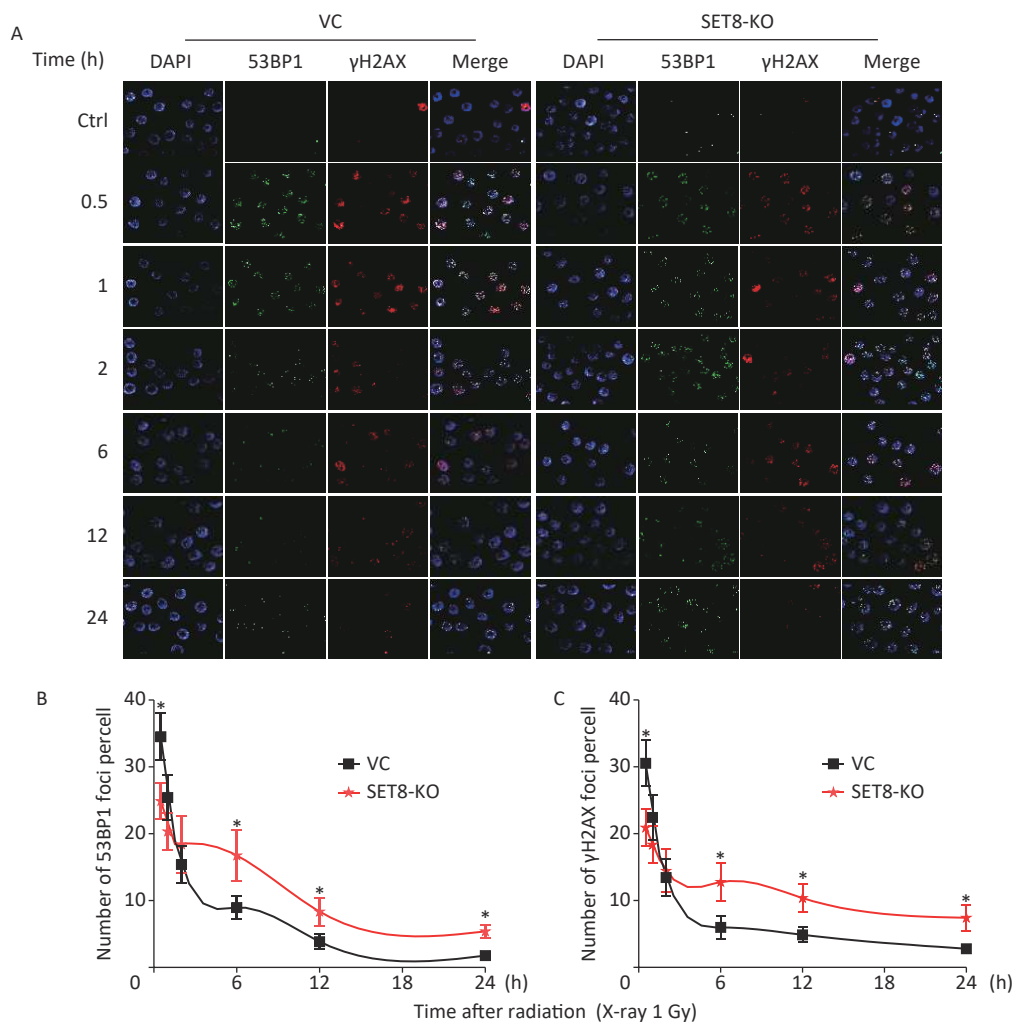


Figure 5. Kinetics process of DNA damage repair in SET8 knockdown A549 cells. (A) Graph shows quantification of 53BP1 and γ H2AX foci in SET8-KO or control A549 cells exposed to 1 Gy X rays. (B) The numbers of 53BP1 foci in 50 cells of each group were counted for each time point. (C) The numbers of γ H2AX foci in 50 cells of each group were counted for each time point. Significance was determined by unpaired *t*-test. * $P < 0.05$. VC, vector control.

H4K20me1 inhibitor, A-196, inhibits 53BP1 foci formation upon ionizing radiation and reduces NHEJ-mediated DNA repair^[37]. In addition, the inhibitor of SET8 (UNC-0379) blocks H4K20 methylation and augments radiosensitivity by reducing recruitment of the 53BP1 protein to DSBs is an effective radiosensitizer of human glioma cells^[38]. Developing SET8/H4K20me1 inhibitors is an effective step toward elucidating the roles of SET8 in DNA repair and appears to be a promising prospect on combination radiotherapy *via* convenient pharmacologic perturbation.

In conclusion, our work and existing reports suggest that the histone methylation pathway, SET8/H4K20me1, which is required for DNA repair, is an important and novel target for the development of radiosensitizers with therapeutic relevance. As new epigenetic inhibitors are synthesized and tested in preclinical and clinical

settings, it will be important to consider combining the epigenetic inhibitors with radiation or other types of DNA-damaging chemotherapy for precise radiotherapy.

CONTRIBUTION

BH and DP contributed to the conception and design of the study. DP, RD, RL, and AS conducted the investigation. DP and BH wrote the first draft of the manuscript. RD, XL, and CL wrote sections and reviewed the manuscript. All authors contributed to the manuscript revision, and read and approved the submitted version.

GRANT SUPPORT

We also appreciate the staff of the Heavy Ion Research Facility in Lanzhou for the offer of $^{12}\text{C}^{6+}$ ion.

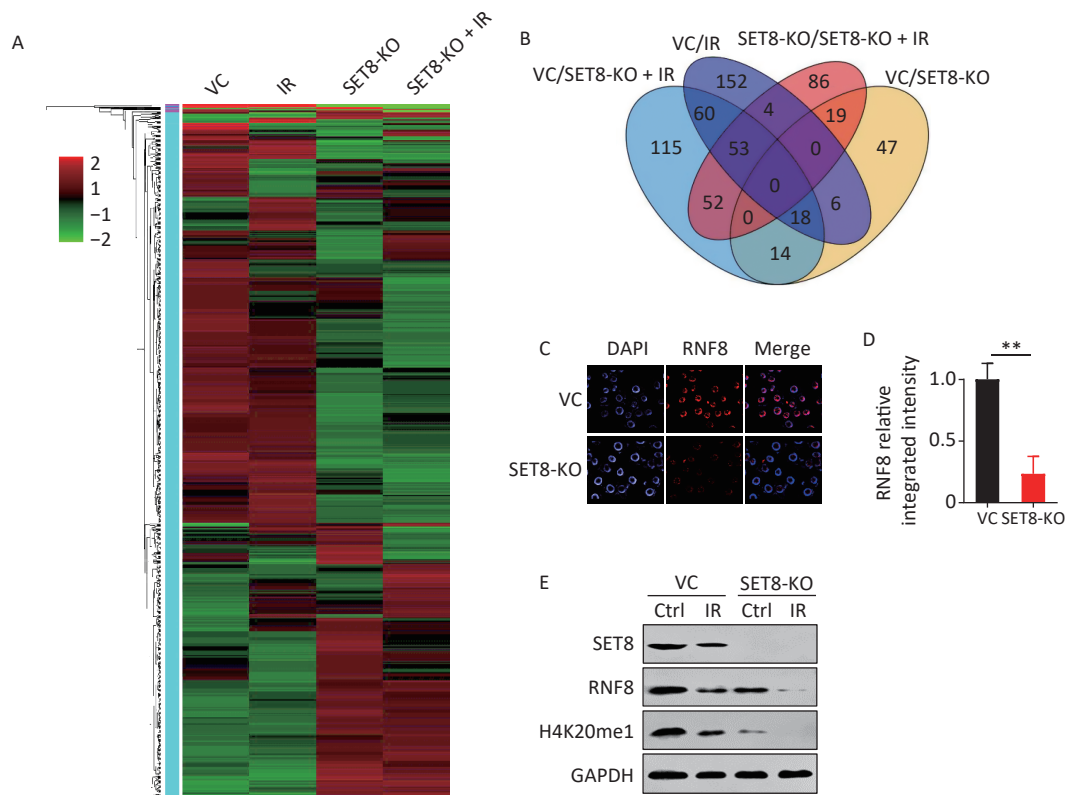


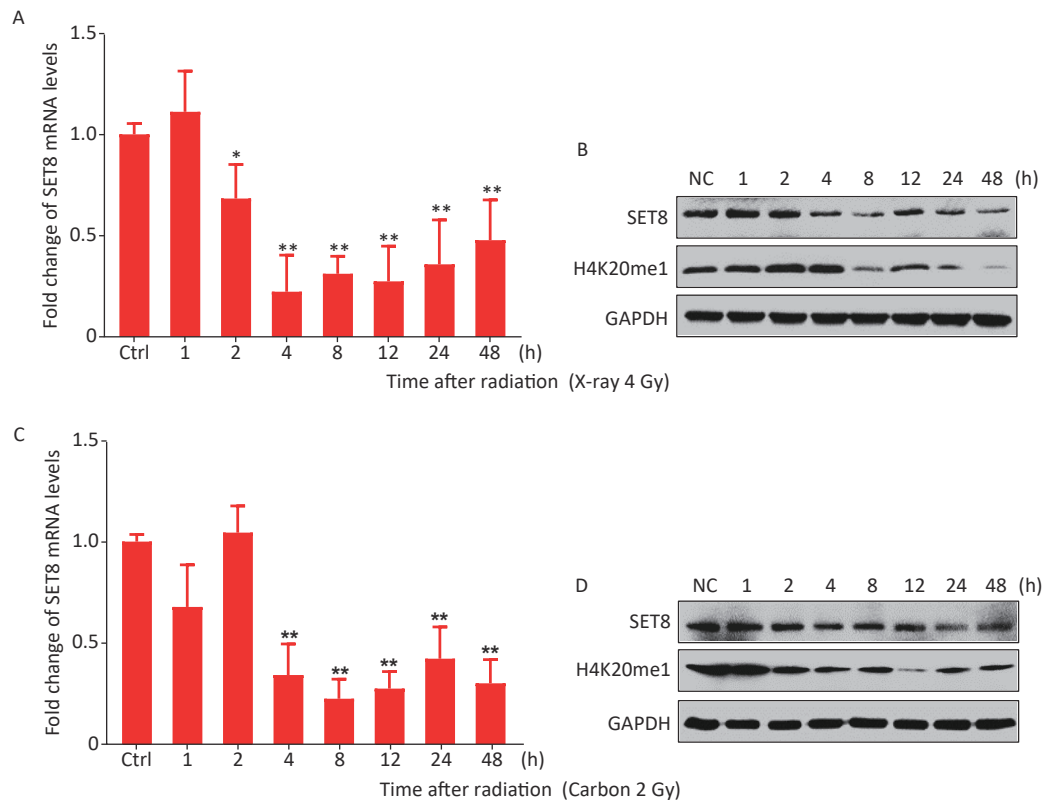
Figure 6. Radiosensitivity in the SET8 alteration A549 and MCF7 cells. (A) Heat map of RNA sequence analysis in vector control (VC) and SET8 KO groups A549 cells, 12 h after 4Gy X-ray radiation. Genes that were significantly differentially expressed ($P < 0.05$) and had greater than 2-fold difference in expression were identified. (B) Venn diagram showing the total number of gene comparisons between different treatments groups. (C) & (D) Representative immunofluorescence images and RNF8 relative integrated immunofluorescence intensity in control and SET8-KO A549 cells. (E) Western blot assay of SET8, RNF8 and H4K20me1 protein levels in SET8-KO or control A549 and MCF7 cells exposed to 4 Gy X rays after 8 h. Significance was determined by unpaired *t*-test in (D). ** $P < 0.01$. IR, irradiation.

Received: July 28, 2021;

Accepted: October 8, 2021

REFERENCES

- Smith RA, Andrews KS, Brooks D, et al. Cancer screening in the United States, 2019: a review of current American Cancer Society guidelines and current issues in cancer screening. *CA Cancer J Clin*, 2019; 69, 184–210.
- Sawan C, Herceg Z. Histone modifications and cancer. *Adv Genet*, 2010; 70, 57–85.
- McCabe MT, Mohammad HP, Barbash O, et al. Targeting histone methylation in cancer. *Cancer J*, 2017; 23, 292–301.
- Nishioka K, Rice JC, Sarma K, et al. PR-Set7 is a nucleosome-specific methyltransferase that modifies lysine 20 of histone H4 and is associated with silent chromatin. *Mol Cell*, 2002; 9, 1201–13.
- Shi XB, Kachirskaia I, Yamaguchi H, et al. Modulation of p53 function by set8-mediated methylation at lysine 382. *Mol Cell*, 2007; 27, 636–46.
- Yu N, Huangyang PW, Yang XH, et al. MicroRNA-7 suppresses the invasive potential of breast cancer cells and sensitizes cells to DNA damages by targeting histone methyltransferase SET8. *J Biol Chem*, 2013; 288, 19633–42.
- Beck DB, Oda H, Shen SS, et al. PR-Set7 and H4K20me1: at the crossroads of genome integrity, cell cycle, chromosome condensation, and transcription. *Genes Dev*, 2012; 26, 325–37.
- Huen MSY, Sy SMH, van Deursen JM, et al. Direct interaction between SET8 and proliferating cell nuclear antigen couples H4-K20 methylation with DNA replication. *J Biol Chem*, 2008; 283, 11073–7.
- Houston SI, McManus KJ, Adams MM, et al. Catalytic function of the PR-Set7 histone H4 lysine 20 monomethyltransferase is essential for mitotic entry and genomic stability. *J Biol Chem*, 2008; 283, 19478–88.
- Jørgensen S, Schotta G, Sørensen CS. Histone H4 lysine 20 methylation: key player in epigenetic regulation of genomic integrity. *Nucleic Acids Res*, 2013; 41, 2797–806.
- Cerami E, Gao JJ, Dogrusoz U, et al. The cBio cancer genomics portal: an open platform for exploring multidimensional cancer genomics data. *Cancer Discov*, 2012; 2, 401–4.
- Hoadley KA, Yau C, Hinoue T, et al. Cell-of-origin patterns dominate the molecular classification of 10, 000 tumors from 33 types of cancer. *Cell*, 2018; 173, 291–304.e6.
- Sanjana NE, Shalem O, Zhang F. Improved vectors and genome-wide libraries for CRISPR screening. *Nat Methods*, 2014; 11, 783–4.
- Puchtler H, Sweat Waldrop F, Conner HM, et al. Carnoy fixation: practical and theoretical considerations. *Histochemie*, 1968; 16, 361–71.
- Hayashi M. The micronucleus test—most widely used *in vivo* genotoxicity test—. *Genes Environ*, 2016; 38, 18.
- Savage JRK. A comment on the quantitative relationship between micronuclei and chromosomal aberrations. *Mutat Res Lett*, 1988; 207, 33–6.
- Yuan HT, Yan M, Zhang GX, et al. CancerSEA: a cancer single-cell state atlas. *Nucleic Acids Res*, 2019; 47, D900–8.
- Kim KT, Lee HW, Lee HO, et al. Single-cell mRNA sequencing identifies subclonal heterogeneity in anti-cancer drug responses of lung adenocarcinoma cells. *Genome Biol*, 2015; 16, 127.
- Guillaumet-Adkins A, Rodríguez-Esteban G, Mereu E, et al. Single-cell transcriptome conservation in cryopreserved cells and tissues. *Genome Biol*, 2017; 18, 45.
- Braune EB, Tsoi YL, Phoon YP, et al. Loss of CSL unlocks a hypoxic response and enhanced tumor growth potential in breast cancer cells. *Stem Cell Reports*, 2016; 6, 643–51.
- Jordan NV, Bardia A, Wittner BS, et al. HER2 expression identifies dynamic functional states within circulating breast cancer cells. *Nature*, 2016; 537, 102–6.
- van Oorschot B, Hovingh SE, Moerland PD, et al. Reduced activity of double-strand break repair genes in prostate cancer patients with late normal tissue radiation toxicity. *Int J Radiat Oncol Biol Phys*, 2014; 88, 664–70.
- Li F, Liu B, Zhou XL, et al. Silencing of E3 ubiquitin ligase RNF8 enhances ionizing radiation sensitivity of medulloblastoma cells by promoting the deubiquitination of PCNA. *Oncol Res*, 2018; 26, 1365–73.
- Pogribny I, Koturbash I, Tryndyak V, et al. Fractionated low-dose radiation exposure leads to accumulation of DNA damage and profound alterations in DNA and histone methylation in the murine thymus. *Mol Cancer Res*, 2005; 3, 553–61.
- Maroschik B, Gürtler A, Krämer A, et al. Radiation-induced alterations of histone post-translational modification levels in lymphoblastoid cell lines. *Radiat Oncol*, 2014; 9, 15.
- Sak A, Kübler D, Bannik K, et al. Dependence of radiation-induced H2AX phosphorylation on histone methylation: evidence from the chromatin immunoprecipitation assay. *Int J Radiat Biol*, 2015; 91, 346–53.
- Game JC, Williamson MS, Spicakova T, et al. The *RAD6/BRE1* histone modification pathway in *Saccharomyces* confers radiation resistance through a *RAD51*-dependent process that is independent of *RAD18*. *Genetics*, 2006; 173, 1951–68.
- Zhang BP, Li B, Cheng JY, et al. Anti-cancer effect of 20(S)-ginsenoside-Rh2 on oral squamous cell carcinoma cells via the decrease in ROS and downregulation of MMP-2 and VEGF. *Biomed Environ Sci*, 2020; 33, 713–7.
- Dai XY, Song AY, Mu L, et al. Potential function of *MMP3* gene in degradation of extracellular matrix complex in colorectal carcinoma. *Biomed Environ Sci*, 2021; 34, 66–70.
- Lu X, Simon MD, Chodaparambil JV, et al. The effect of H3K79 dimethylation and H4K20 trimethylation on nucleosome and chromatin structure. *Nat Struct Mol Biol*, 2008; 15, 1122–4.
- Dulev S, Tkach J, Lin SC, et al. SET8 methyltransferase activity during the DNA double-strand break response is required for recruitment of 53BP1. *EMBO Rep*, 2014; 15, 1163–74.
- Gursoy-Yuzugullu O, House N, Price BD. Patching broken DNA: nucleosome dynamics and the repair of DNA breaks. *J Mol Biol*, 2016; 428, 1846–60.
- Zhao MJ, Song YF, Niu HT, et al. Adenovirus-mediated downregulation of the ubiquitin ligase RNF8 sensitizes bladder cancer to radiotherapy. *Oncotarget*, 2016; 7, 8956–67.
- Tan XH, Peng J, Fu YB, et al. miR-638 mediated regulation of *BRCA1* affects DNA repair and sensitivity to UV and cisplatin in triple-negative breast cancer. *Breast Cancer Res*, 2014; 16, 435.
- Zhou HX, Mu XQ, Chen J, et al. RNAi silencing targeting RNF8 enhances radiosensitivity of a non-small cell lung cancer cell line A549. *Int J Radiat Biol*, 2013; 89, 708–15.
- Blum G, Ibáñez G, Rao XJ, et al. Small-molecule inhibitors of SETD8 with cellular activity. *ACS Chem Biol*, 2014; 9, 2471–8.
- Bromberg KD, Mitchell TRH, Upadhyay AK, et al. The SUV4-20 inhibitor A-196 verifies a role for epigenetics in genomic integrity. *Nat Chem Biol*, 2017; 13, 317–24.
- Gursoy-Yuzugullu O, Carman C, Serafim RB, et al. Epigenetic therapy with inhibitors of histone methylation suppresses DNA damage signaling and increases glioma cell radiosensitivity. *Oncotarget*, 2017; 8, 24518–32.



Supplementary Figure S1. SET8 expressions and H4K20me1 dynamic changes after X-ray or carbon ion radiation. (A) Relative SET8 mRNA expression was measured by qRT-PCR at indicated time points in A549 cells after 4 Gy X-ray irradiation. GAPDH was used as internal controls. (B) SET8 and H4K20me1 levels in A549 cells at indicated time points after 4 Gy X-ray radiation were measured by western blot assay. (C) Relative SET8 mRNA expression was measured by qRT-PCR at indicated time points in A549 cells after 2 Gy Carbon irradiation. (D) SET8 and H4K20me1 levels in A549 cells at indicated time points after 2 Gy Carbon radiation were measured by western blot assay. Significance was determined by unpaired *t*-test. **P* < 0.05; ***P* < 0.01.

Supplementary Table S1. sgRNA used in CRISPR/Cas9 knockout experiments

Target	Sequence (5'-3')
Human-SET8-sg1	TTTAGGAGAACGTATTTACC
Human-SET8-sg2	GCACGTGACTACCTGCAGCT
Mouse-SET8-sg1	AGTATCTGAGCAAAACCTAC
Mouse-SET8-sg1	TCCGGAACTCCTCCGCACA

Supplementary Table S2. Oligonucleotide primers for qRT-PCR

Genes	Upstream primer (5'-3')	Downstream primer (5'-3')
SET8	CGCAAACCTACGGATTTC	CGATGAGGTC AATCTTCATT
GAPDH	GTCTCTCTGACTTCAACAGCG	ACCACCTGTTGCTGTAGCCAA

Supplementary Table S3. Gene expression signatures in SET8-KO A549 cells

Seq_id	(VC) fpkm	(KO)3_7_fpkm	log2FC(KO/VC)	Regulate	Description
ENSG00000264148	0	49.1764	5.61989422	up	-
ENSG00000236991	0.330355	3.76492	3.510530124	up	-
ENSG00000088448	41.5497	364.193	3.131793228	up	ankyrin repeat domain 10 [Source:HGNC Symbol;Acc:20265]
ENSG00000185437	0	8.08694	3.015593908	up	SH3 domain binding glutamic acid-rich protein [Source:HGNC Symbol;Acc:10822]
ENSG00000228950	0	7.66067	2.937470575	up	-
ENSG00000271267	0	5.72202	2.51652454	up	-
ENSG00000232859	1.14869	6.19551	2.43123354	up	LYR motif containing 9 [Source:HGNC Symbol;Acc:27314]
ENSG00000172339	1.08544	5.63913	2.377192622	up	asparagine-linked glycosylation 14 homolog (S. cerevisiae) [Source:HGNC Symbol;Acc:28287]
ENSG00000213420	1.27423	5.78869	2.183611189	up	glypican 2 [Source:HGNC Symbol;Acc:4450]
ENSG00000131095	0.961888	4.15931	2.112403391	up	glial fibrillary acidic protein [Source:HGNC Symbol;Acc:4235]
ENSG00000185920	3.25398	13.6198	2.065428229	up	patched 1 [Source:HGNC Symbol;Acc:9585]
ENSG00000234160	0	3.97046	1.989306161	up	-
ENSG00000241769	1.82417	7.01286	1.942762742	up	-
ENSG00000153291	1.65069	6.24826	1.92038528	up	solute carrier family 25, member 27 [Source:HGNC Symbol;Acc:21065]
ENSG00000254335	0	3.74532	1.905088988	up	cadherin 12 (N-cadherin 2) pseudogene 1 [Source:HGNC Symbol;Acc:37698]
ENSG00000230438	1.00366	3.68563	1.876640622	up	-
ENSG00000170899	1.78022	5.97155	1.746049911	up	glutathione S-transferase alpha 4 [Source:HGNC Symbol;Acc:4629]
ENSG00000104205	1.80144	5.94424	1.722341765	up	serum/glucocorticoid regulated kinase family, member 3 [Source:HGNC Symbol;Acc:10812]
ENSG00000139946	1.0563	3.48076	1.72038271	up	pellino E3 ubiquitin protein ligase family member 2 [Source:HGNC Symbol;Acc:8828]
ENSG00000137843	1.61001	5.23319	1.70062099	up	p21 protein (Cdc42/Rac)-activated kinase 6 [Source:HGNC Symbol;Acc:16061]
ENSG00000246273	6.43651	18.854	1.550520085	up	SBF2 antisense RNA 1 [Source:HGNC Symbol;Acc:27438]
ENSG00000176371	3.07709	8.49372	1.464829909	up	zinc finger and SCAN domain containing 2 [Source:HGNC Symbol;Acc:20994]
ENSG00000080298	1.3528	3.72538	1.461439027	up	regulatory factor X, 3 (influences HLA class II expression) [Source:HGNC Symbol;Acc:9984]
ENSG00000133794	5.24692	13.2361	1.334935398	up	aryl hydrocarbon receptor nuclear translocator-like [Source:HGNC Symbol;Acc:701]
ENSG00000111850	2.28058	5.72774	1.328565227	up	small integral membrane protein 8 [Source:HGNC Symbol;Acc:21401]
ENSG00000126070	4.95836	12.1416	1.292023623	up	eukaryotic translation initiation factor 2C, 3 [Source:HGNC Symbol;Acc:18421]
ENSG00000154781	6.58946	15.389	1.223667339	up	coiled-coil domain containing 174 [Source:HGNC Symbol;Acc:28033]
ENSG00000111490	5.02417	11.7049	1.220155423	up	TBC1 domain family, member 30 [Source:HGNC Symbol;Acc:29164]
ENSG00000112183	2.14386	4.84626	1.17666111	up	RNA binding motif protein 24 [Source:HGNC Symbol;Acc:21539]
ENSG00000162433	5.88931	13.2923	1.174420239	up	adenylate kinase 4 [Source:HGNC Symbol;Acc:363]
ENSG00000189144	3.3689	7.60021	1.173761677	up	zinc finger protein 573 [Source:HGNC Symbol;Acc:26420]
ENSG00000267100	1.88424	4.19986	1.156358501	up	ILF3 antisense RNA 1 (head to head) [Source:HGNC Symbol;Acc:27115]
ENSG00000147654	6.32929	13.8479	1.129551635	up	estrogen receptor binding site associated, antigen, 9 [Source:HGNC Symbol;Acc:3123]
ENSG00000180447	1.91579	4.12663	1.107024662	up	growth arrest-specific 1 [Source:HGNC Symbol;Acc:4165]
ENSG00000254870	17.3676	37.3119	1.103237423	up	ATP6V1G2-DDX39B readthrough (non-protein coding) [Source:HGNC Symbol;Acc:41999]

Continued

Seq_id	(VC) fpkm	(KO)3_7_fpkm	log2FC(KO/VC)	Regulate	Description
ENSG00000143622	14.5221	30.7865	1.08404777	up	Ras-like without CAAX 1 [Source:HGNC Symbol;Acc:10023]
ENSG00000168283	5.71889	12.116	1.083106422	up	BMI1 polycomb ring finger oncogene [Source:HGNC Symbol;Acc:1066]
ENSG00000178537	8.94604	18.9266	1.081094153	up	solute carrier family 25 (carnitine/acylcarnitine translocase), member 20 [Source:HGNC Symbol;Acc:1421]
ENSG00000047617	6.34087	13.2084	1.058703012	up	anoctamin 2 [Source:HGNC Symbol;Acc:1183]
ENSG00000160404	9.5724	19.6562	1.038031853	up	torsin family 2, member A [Source:HGNC Symbol;Acc:11996]
ENSG00000116711	2.30078	4.72253	1.037436921	up	phospholipase A2, group IVA (cytosolic, calcium-dependent) [Source:HGNC Symbol;Acc:9035]
ENSG00000183579	1.75972	3.58008	1.024645935	up	zinc and ring finger 3 [Source:HGNC Symbol;Acc:18126]
ENSG00000197415	5.96185	12.0142	1.010908603	up	ventricular zone expressed PH domain-containing 1 [Source:HGNC Symbol;Acc:25735]
ENSG00000198088	17.2525	8.51158	-1.019306564	down	nucleoporin 62kDa C-terminal like [Source:HGNC Symbol;Acc:25960]
ENSG00000179046	10.0612	4.93927	-1.026432646	down	tripartite motif family-like 2 [Source:HGNC Symbol;Acc:26378]
ENSG00000085117	16.3935	8.02257	-1.030987524	down	CD82 molecule [Source:HGNC Symbol;Acc:6210]
ENSG00000270882	13.1691	6.38904	-1.043485676	down	-
ENSG00000167535	11.2491	5.40623	-1.057114786	down	calcium channel, voltage-dependent, beta 3 subunit [Source:HGNC Symbol;Acc:1403]
ENSG00000187764	5.71625	2.7422	-1.059735217	down	sema domain, immunoglobulin domain (Ig), transmembrane domain (TM) and short cytoplasmic domain, (semaphorin) 4D [Source:HGNC Symbol;Acc:10732]
ENSG00000115421	11.6833	5.54962	-1.073986933	down	poly(A) polymerase gamma [Source:HGNC Symbol;Acc:14982]
ENSG00000115947	25.359	11.9667	-1.083472494	down	origin recognition complex, subunit 4 [Source:HGNC Symbol;Acc:8490]
ENSG00000168143	4.12583	1.93689	-1.090942355	down	family with sequence similarity 83, member B [Source:HGNC Symbol;Acc:21357]
ENSG00000137868	4.36322	2.03399	-1.101080632	down	stimulated by retinoic acid 6 [Source:HGNC Symbol;Acc:30650]
ENSG00000184517	11.179	5.18427	-1.108578378	down	ZFP1 zinc finger protein [Source:HGNC Symbol;Acc:23328]
ENSG00000166025	8.62556	3.98626	-1.113582313	down	angiominin like 1 [Source:HGNC Symbol;Acc:17811]
ENSG00000164506	6.06679	2.79463	-1.118276086	down	syntaxin binding protein 5 (tomosyn) [Source:HGNC Symbol;Acc:19665]
ENSG00000131374	8.96638	4.11688	-1.122974246	down	TBC1 domain family, member 5 [Source:HGNC Symbol;Acc:19166]
ENSG00000157514	13.3161	6.03102	-1.142697685	down	TSC22 domain family, member 3 [Source:HGNC Symbol;Acc:3051]
ENSG00000204396	11.6324	5.11676	-1.184846314	down	von Willebrand factor A domain containing 7 [Source:HGNC Symbol;Acc:13939]
ENSG00000114861	7.03474	3.06923	-1.196620342	down	forkhead box P1 [Source:HGNC Symbol;Acc:3823]
ENSG00000164808	46.0156	20.0548	-1.198175461	down	KIAA0146 [Source:HGNC Symbol;Acc:28971]
ENSG00000281181	16.7705	7.1703	-1.225820316	down	-
ENSG00000167081	8.3093	3.50186	-1.246605537	down	pre-B-cell leukemia homeobox 3 [Source:HGNC Symbol;Acc:8634]
ENSG00000214174	4.86578	2.03253	-1.259394446	down	archaelysin family metalloproteinase 2 pseudogene 1 [Source:HGNC Symbol;Acc:26491]
ENSG00000072195	8.30099	3.33036	-1.317605271	down	SPEG complex locus [Source:HGNC Symbol;Acc:16901]
ENSG00000109458	3.66758	1.44769	-1.34107573	down	GRB2-associated binding protein 1 [Source:HGNC Symbol;Acc:4066]
ENSG00000075043	5.86368	2.26188	-1.374283981	down	potassium voltage-gated channel, KQT-like subfamily, member 2 [Source:HGNC Symbol;Acc:6296]

Continued

Seq_id	(VC) fpkm	(KO)3_7_fpkm	log2FC(KO/VC)	Regulate	Description
ENSG00000131746	9.23984	3.52582	-1.389909046	down	tensin 4 [Source:HGNC Symbol;Acc:24352]
ENSG00000156453	4.01672	1.50392	-1.417290071	down	protocadherin 1 [Source:HGNC Symbol;Acc:8655]
ENSG00000188517	6.04896	2.24749	-1.428372424	down	collagen, type XXV, alpha 1 [Source:HGNC Symbol;Acc:18603]
ENSG00000265096	8.69038	3.22807	-1.428747399	down	Uncharacterized protein [Source:UniProtKB/TrEMBL;Acc:J3KS61]
ENSG00000151689	9.40788	3.47631	-1.436312918	down	inositol polyphosphate-1-phosphatase [Source:HGNC Symbol;Acc:6071]
ENSG00000088756	4.70196	1.68862	-1.477417559	down	Rho GTPase activating protein 28 [Source:HGNC Symbol;Acc:25509]
ENSG00000104081	5.96943	2.12103	-1.492828154	down	Bcl2 modifying factor [Source:HGNC Symbol;Acc:24132]
ENSG00000118194	4.6428	1.62065	-1.518422578	down	troponin T type 2 (cardiac) [Source:HGNC Symbol;Acc:11949]
ENSG00000188266	6.21225	2.05372	-1.596876388	down	aminoglycoside phosphotransferase domain containing 1 [Source:HGNC Symbol;Acc:34403]
ENSG00000172927	9.72759	3.20937	-1.599792299	down	myeloma overexpressed (in a subset of t(11;14) positive multiple myelomas) [Source:HGNC Symbol;Acc:7563]
ENSG00000278932	9.65933	3.14891	-1.617070599	down	-
ENSG00000107614	3.78983	1.11699	-1.762516865	down	tRNA aspartic acid methyltransferase 1 [Source:HGNC Symbol;Acc:2977]
ENSG00000152076	3.91793	1.15134	-1.766777686	down	coiled-coil domain containing 74B [Source:HGNC Symbol;Acc:25267]
ENSG00000159788	5.99872	1.73903	-1.786371872	down	regulator of G-protein signaling 12 [Source:HGNC Symbol;Acc:9994]
ENSG00000232973	5.70581	1.57831	-1.85405111	down	CYP1B1 antisense RNA 1 [Source:HGNC Symbol;Acc:28543]
ENSG00000067141	4.28714	1.16488	-1.879834187	down	neogenin 1 [Source:HGNC Symbol;Acc:7754]
ENSG00000203326	25.5951	6.93345	-1.884222339	down	zinc finger protein 525 [Source:HGNC Symbol;Acc:29423]
ENSG00000163995	4.71407	1.25699	-1.907000009	down	actin binding LIM protein family, member 2 [Source:HGNC Symbol;Acc:19195]
ENSG00000280130	3.76176	0	-1.911407808	down	-
ENSG00000240364	3.86536	0	-1.950602786	down	ribosomal protein L31 pseudogene 59 [Source:HGNC Symbol;Acc:36975]
ENSG00000174640	4.63741	1.17475	-1.980965515	down	solute carrier organic anion transporter family, member 2A1 [Source:HGNC Symbol;Acc:10955]
ENSG00000133401	4.00349	0.995203	-2.008195463	down	PDZ domain containing 2 [Source:HGNC Symbol;Acc:18486]
ENSG00000278903	11.7426	2.82235	-2.056783067	down	-
ENSG00000204406	6.34622	1.49977	-2.081156265	down	methyl-CpG binding domain protein 5 [Source:HGNC Symbol;Acc:20444]
ENSG00000280987	8.10572	1.90811	-2.086795997	down	-
ENSG00000108387	7.70484	1.56887	-2.296039185	down	septin 4 [Source:HGNC Symbol;Acc:9165]
ENSG00000253492	5.21647	0	-2.383073861	down	cadherin 12 (N-cadherin 2) pseudogene 3 [Source:HGNC Symbol;Acc:37699]
ENSG00000184271	7.99757	1.44707	-2.466427003	down	POU class 6 homeobox 1 [Source:HGNC Symbol;Acc:9224]
ENSG00000249684	5.82118	0	-2.541311629	down	-
ENSG00000185324	207.869	31.9115	-2.703526292	down	cyclin-dependent kinase 10 [Source:HGNC Symbol;Acc:1770]
ENSG00000251141	12.3399	1.88182	-2.71313016	down	-
ENSG00000130208	6.13461	0.690214	-3.151855987	down	apolipoprotein C-I [Source:HGNC Symbol;Acc:607]
ENSG00000270808	9.54955	0	-3.255432751	down	-
ENSG00000257341	6.31322	0.598144	-3.399811274	down	-
ENSG00000266210	11.7633	0	-3.556220936	down	Metazoan signal recognition particle RNA [Source:RFAM;Acc:RF00017]
ENSG00000189283	15.9633	0.425823	-5.228361236	down	fragile histidine triad [Source:HGNC Symbol;Acc:3701]
ENSG00000277739	85.2919	0	-6.414336833	down	-